

2012

## **B and B-s meson decay constants from lattice QCD**

Heechang Na

Junko Shigemitsu

Chris J. Monahan

*William & Mary*, [cjmonahan@wm.edu](mailto:cjmonahan@wm.edu)

Christine T. H. Davies

Follow this and additional works at: <https://scholarworks.wm.edu/aspubs>

---

### **Recommended Citation**

Na, H., Monahan, C. J., Davies, C. T., Horgan, R., Lepage, G. P., Shigemitsu, J., & HPQCD Collaboration. (2012). B and B s meson decay constants from lattice QCD. *Physical Review D*, 86(3), 034506.

This Article is brought to you for free and open access by the Arts and Sciences at W&M ScholarWorks. It has been accepted for inclusion in Arts & Sciences Articles by an authorized administrator of W&M ScholarWorks. For more information, please contact [scholarworks@wm.edu](mailto:scholarworks@wm.edu).

**$B$  and  $B_s$  meson decay constants from lattice QCD**Heechang Na,<sup>1,\*</sup> Chris J. Monahan,<sup>2</sup> Christine T. H. Davies,<sup>3</sup> Ron Horgan,<sup>4</sup>  
G. Peter Lepage,<sup>5</sup> and Junko Shigemitsu<sup>1</sup>

(HPQCD Collaboration)

<sup>1</sup>*Department of Physics, The Ohio State University, Columbus, Ohio 43210, USA*<sup>2</sup>*Department of Physics, College of William and Mary, Virginia 23187-8795, USA*<sup>3</sup>*SUPA, School of Physics and Astronomy, University of Glasgow, Glasgow G12 8QQ, United Kingdom*<sup>4</sup>*DAMTP, Cambridge University, CB3 0WA, United Kingdom*<sup>5</sup>*Laboratory of Elementary Particle Physics, Cornell University, Ithaca, New York 14853, USA*

(Received 26 February 2012; published 21 August 2012)

We present a new determination of the  $B$  and  $B_s$  meson decay constants using nonrelativistic quantum chromodynamics (NRQCD)  $b$ -quarks, highly improved staggered quark (HISQ) light and strange valence quarks and the MILC collaboration  $N_f = 2 + 1$  lattices. The new calculations improve on HPQCD's earlier work with NRQCD  $b$ -quarks by replacing AsqTad with HISQ valence quarks, by including a more chiral MILC fine ensemble in the analysis, and by employing better tuned quark masses and overall scale. We find  $f_B = 0.191(9)$  GeV,  $f_{B_s} = 0.228(10)$  GeV and  $f_{B_s}/f_B = 1.188(18)$ . Combining the new value for  $f_{B_s}/f_B$  with a recent very precise determination of the  $B_s$  meson decay constant based on HISQ  $b$ -quarks,  $f_{B_s} = 0.225(4)$  GeV, leads to  $f_B = 0.189(4)$  GeV. With errors of just 2.1% this represents the most precise  $f_B$  available today.

DOI: [10.1103/PhysRevD.86.034506](https://doi.org/10.1103/PhysRevD.86.034506)

PACS numbers: 12.38.Gc

**I. INTRODUCTION**

Precision electroweak data gathered at the  $B$  factories, the Tevatron and at LHCb are allowing particle physicists to carry out stringent tests of the Standard Model (SM) and search for hints of new physics (NP). Several groups, for instance, are studying global fits to the Cabibbo-Kobayashi-Maskawa unitarity triangle (UT) and checking whether various combinations of constraints coming from experiment and theory can be accommodated consistently with each other [1–3]. In recent years some tensions at the 2–3  $\sigma$  level within the SM have emerged from these studies and it will be very interesting to see whether future improvements in experimental and theory inputs will remove these tensions or conversely elevate them to serious hints of new physics.

Lattice quantum chromodynamics (QCD) is playing an important role in UT analyses, providing crucial inputs such as  $\epsilon_K$ ,  $\hat{B}_{B_q}$ ,  $\xi = f_{B_s}\sqrt{M_{B_s}}/f_B\sqrt{M_B}$ ,  $f_B$  and information on semileptonic form factors [4]. To make progress in resolving the tensions in UT analyses it is imperative to reduce the errors in current lattice results. In Ref. [1] the  $B$  meson decay constant  $f_B$  is not used as an input for the global fits but becomes instead one of the fit outputs  $f_B^{(\text{fit})}$ . This  $f_B^{(\text{fit})}$  is then compared with the SM (i.e., lattice QCD) value  $f_B^{(\text{QCD})}$  to check for consistency. The authors of Ref. [1] experiment with dropping different processes in

their global fits and study how this affects  $f_B^{(\text{fit})}$  and when  $f_B^{(\text{fit})}$  agrees best with  $f_B^{(\text{QCD})}$ . Using this fit-comparison procedure, the authors attempt to determine the dominant source of deviations from the SM, e.g., whether it is coming from  $B \rightarrow \psi K_s(\sin 2\beta)$ ,  $B_s$  and  $B_d$  mixing, Kaon mixing ( $\epsilon_K$ ) or  $B \rightarrow \tau\nu$ . Needless to say this  $f_B^{(\text{fit})} - f_B^{(\text{QCD})}$  comparison method requires knowing  $f_B^{(\text{QCD})}$  as accurately as possible. In this article we significantly reduce errors in  $f_B^{(\text{QCD})}$ . With reduced errors, the  $B$  meson decay constant will hopefully help further constrain UT analyses in the future.

In the next section we introduce the lattice setup and explain how the bottom and strange quark masses were fixed in our lattice actions. Section III discusses operator matching between heavy-light currents in full continuum QCD and in the lattice theory. We describe two-point correlators and the smearings employed. In Sec. IV we present our fitting strategies to the two-point correlators and describe how the extracted amplitudes lead to the hadronic matrix elements relevant for determining decay constants. This section also includes summary tables of fit results for  $\Phi_s = f_{B_s}\sqrt{M_{B_s}}$ ,  $\Phi = f_B\sqrt{M_B}$ , and their ratios for each of the 6 MILC ensembles that we work with. Then in Sec. V we explain how continuum and chiral limit physics is extracted from our simulation data. Section VI discusses results at the physical point and the error budget and we conclude with a summary in Sec. VII. For the rest of this article we omit the “QCD” in  $f_B^{(\text{QCD})}$ .

\*Present address: Argonne Leadership Computing Facility, Argonne National Laboratory, Argonne, IL 60439, USA.

## II. THE LATTICE SETUP AND TUNING OF BARE QUARK MASSES

HPQCD's previous work on  $B$  and  $B_s$  meson decay constants with nonrelativistic quantum chromodynamics (NRQCD)  $b$ -quarks used AsqTad light and strange quarks [5]. It utilized the MILC AsqTad  $N_f = 2 + 1$  lattices [6]. In the present work we replace the AsqTad valence quarks by their highly improved staggered quark (HISQ) [7] counterparts thereby reducing the dominant discretization errors coming from staggered taste breaking by roughly a factor of three [8]. Details of the MILC ensembles employed here are given in Table I. There is considerable overlap between the MILC ensembles used in the present article and in Ref. [5]. In Ref. [5] an additional coarse ensemble with sea quark masses  $m_l/m_s = 0.007/0.05$  was employed. Here we have added instead a third, more-chiral fine ensemble, the  $40^3 \times 96$  Set F0 with  $m_l/m_s = 0.0031/0.031$ .

For the  $b$ -quarks in our simulations we use the same NRQCD action employed in Ref. [5]. Since the publication of Ref. [5] the HPQCD collaboration has updated the value of the scale parameter  $r_1$  to  $r_1 = 0.3133(23)$  fm [9], and this necessitated a retuning of all quark masses including the bare  $b$ -quark mass  $aM_b$  for all MILC ensembles in Table I. To fix  $aM_b$  we use the spin averaged  $Y$  mass. One calculates,

$$\bar{M}_{b\bar{b}} \equiv \frac{1}{4}[3M_{\text{kin}}(^3S_1) + M_{\text{kin}}(^1S_0)], \quad (1)$$

with

$$M_{\text{kin}} = \frac{p^2 - \Delta E_p^2}{2\Delta E_p}, \quad \Delta E_p = E(p) - E(0), \quad (2)$$

and compares with the experimental value (adjusted for the absence of electromagnetic, annihilation and sea charm quark effects in our simulations) of 9.450(4) GeV [10]. Results from this tuning are shown in Fig. 1. Errors in the data points include statistical and  $r_1/a$  errors. One sees that these are much smaller than the 0.7% error in the absolute physical value of  $r_1$ . To achieve such small statistical errors in  $M_{\text{kin}}$  it was crucial to employ random wall sources for the NRQCD  $b$ -quark propagators. Most of the tuning of  $aM_b$  was carried out with momentum  $2\pi/(aL)$  for

TABLE I. Simulation details on three ‘‘coarse’’ and three ‘‘fine’’ MILC ensembles.

Set	$r_1/a$	$m_l/m_s$ (sea)	$N_{\text{conf}}$	$N_{\text{tsrc}}$	$L^3 \times N_t$
C1	2.647	0.005/0.050	1200	2	$24^3 \times 64$
C2	2.618	0.010/0.050	1200	2	$20^3 \times 64$
C3	2.644	0.020/0.050	600	2	$20^3 \times 64$
F0	3.695	0.0031/0.031	600	4	$40^3 \times 96$
F1	3.699	0.0062/0.031	1200	4	$28^3 \times 96$
F2	3.712	0.0124/0.031	600	4	$28^3 \times 96$

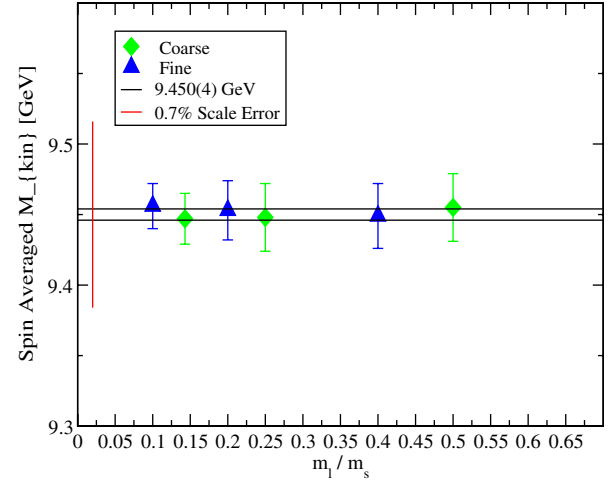


FIG. 1 (color online). Tuning of the  $b$ -quark mass via the spin averaged  $Y$  mass. 9.450 GeV corresponds to the experimental value adjusted for lack of electromagnetic, annihilation and sea charm quark effects in the simulations.

ensembles C1, C2, C3, F1 and F2, and with momentum  $4\pi/(aL)$  for ensemble F0. However, we have checked on one ensemble that consistent  $M_{\text{kin}}$  values result from higher (but not too large) momenta as well. For instance on C2 with  $aM_b = 2.8$  (slightly larger than the actual physical  $b$ -quark mass) one finds  $aM_{\text{kin}}(^3S_1) = 5.933(15)$  for momentum  $2\pi/(aL)$  and  $aM_{\text{kin}}(^3S_1) = 5.941(15)$  for momentum  $4\pi/(aL)$ .

The  $s$ -quark mass was tuned to the (fictitious)  $\eta_s$  mass of 0.6858(40) GeV [9]. Figure 2 shows results for this tuning. All but the set F0 point (most chiral point on plot) were fixed already in Ref. [11]. Having fixed the bottom and strange quark masses on each ensemble one can investigate the mass combination  $M_{B_s} - \bar{M}_{b\bar{b}}/2$ . The leading dependence on the heavy quark mass cancels in this difference,

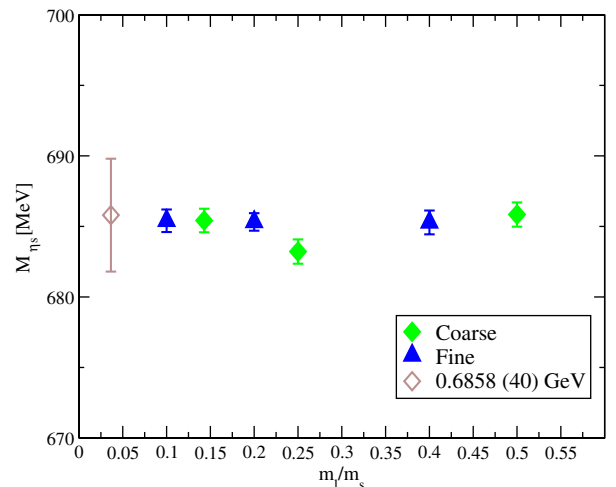


FIG. 2 (color online). Tuning of the strange quark mass via the fictitious  $\eta_s$  meson.

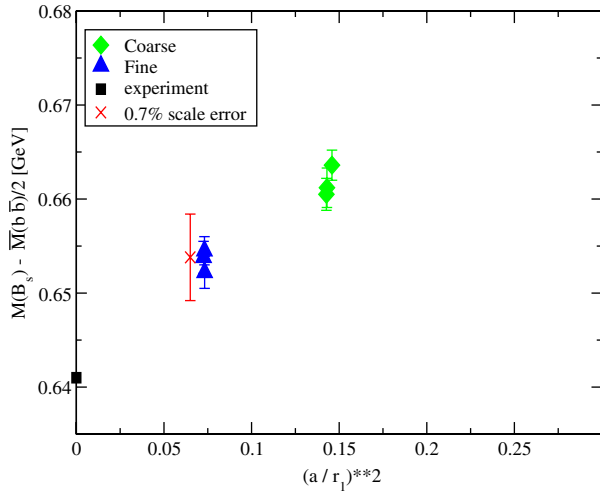


FIG. 3 (color online). The mass difference  $M_{B_s} - \bar{M}_{b\bar{b}}/2$ .

so one is testing how well the lattice actions are simulating QCD bound state dynamics. Results for this mass difference are shown in Fig. 3. Within the  $r_1$  scale error and additional  $\sim 10$  MeV uncertainty from relativistic corrections to  $\bar{M}_{b\bar{b}}$  one sees agreement with experiment after removing discretization effects.

Table II summarizes the valence quark masses used in this article. We include the HISQ valence charm quark masses for each ensemble, since these provide a convenient scale in the chiral extrapolations of Sec. V. The charm quark masses were fixed by tuning to the  $\eta_c$  mass. The light HISQ valence quark mass  $m_l$  is chosen so that  $m_l(\text{valence})/m_s(\text{valence})$  is close to  $m_l(\text{sea})/m_s^{\text{phys}}(\text{AsqTad})$ , where  $m_s^{\text{phys}}(\text{AsqTad})$  corresponds to the physical AsqTad strange quark mass. As a final consistency check of our lattice setup, we have looked at the  $B_s - B$  mass difference. This is shown in Fig. 4.

### III. OPERATOR MATCHING AND RELEVANT CORRELATORS

Decay constants  $f_{B_q}$  are determined by calculating the matrix element of the heavy-light axial vector current  $A_\mu$  between the  $B_q$  meson and hadronic vacuum states. For the temporal component in the  $B_q$  rest frame one has

TABLE II. Valence quark masses.

Set	$am_l$	$am_s$	$am_c$	$aM_b$
C1	0.0070	0.0489	0.6207	2.650
C2	0.0123	0.0492	0.6300	2.688
C3	0.0246	0.0491	0.6235	2.650
F0	0.00339	0.0339	0.4130	1.832
F1	0.00674	0.0337	0.4130	1.832
F2	0.0135	0.0336	0.4120	1.826

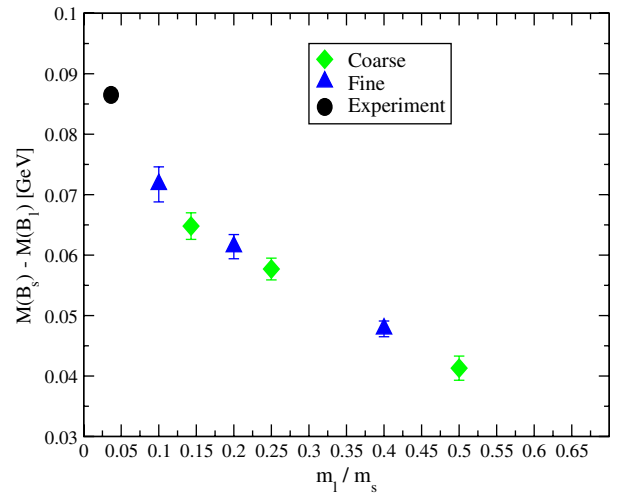


FIG. 4 (color online). The  $B_s - B$  mass difference  $\Delta M$  versus the light valence quark mass.

$$\langle 0|A_0|B_q\rangle_{\text{QCD}} = M_{B_q} f_{B_q}. \quad (3)$$

Simulations are carried out with effective lattice theory currents,

$$J_0^{(0)}(x) = \bar{\Psi}_q \Gamma_0 \Psi_Q, \quad (4)$$

$$J_0^{(1)}(x) = \frac{-1}{2M_b} \bar{\Psi}_q \Gamma_0 \gamma \cdot \nabla \Psi_Q, \quad (5)$$

$$J_0^{(2)}(x) = \frac{-1}{2M_b} \bar{\Psi}_q \gamma \cdot \overleftarrow{\nabla} \gamma_0 \Gamma_0 \Psi_Q, \quad (6)$$

with  $\Gamma_0 = \gamma_5 \gamma_0$  for decay constant calculations.  $\Psi_q$  is the HISQ action light or strange quark field (in its four component “naive fermion” form) and  $\Psi_Q$  is the heavy quark field with the upper two components given by the two-component NRQCD fields and the lower two components set equal to zero. We have matched these effective theory currents to  $A_0$  in full QCD at one-loop through order  $\alpha_s$ ,  $\frac{\Lambda_{\text{QCD}}}{M}$ ,  $\frac{\alpha_s}{aM}$ ,  $a\alpha_s$ ,  $\alpha_s \frac{\Lambda_{\text{QCD}}}{M}$ . Details of the matching of NRQCD/HISQ currents will be presented in a separate publication [12]. The calculations follow the strategy developed in Ref. [13] and employed for NRQCD/AsqTad currents in Ref. [14]. One finds

$$\langle A_0 \rangle_{\text{QCD}} = (1 + \alpha_s \rho_0) \langle J_0^{(0)} \rangle + (1 + \alpha_s \rho_1) \langle J_0^{(1),\text{sub}} \rangle + \alpha_s \rho_2 \langle J_0^{(2),\text{sub}} \rangle, \quad (7)$$

$$J_0^{(i),\text{sub}} = J_0^{(i)} - \alpha_s \zeta_{10} J_0^{(0)}. \quad (8)$$

Here  $\rho_0$ ,  $\rho_1$ ,  $\rho_2$  and  $\zeta_{10}$  are the one-loop matching coefficients.

We use smeared heavy-light bilinears to represent the  $B_q$  mesons. For instance, we create a meson at time  $t_0$  via

$$\Phi_\alpha(\vec{x}, t_0) \equiv \sum_{\vec{x}_1} \bar{\Psi}_Q(\vec{x}_1, t_0) \sigma_\alpha(\vec{x}_1 - \vec{x}) \Gamma_{sc} \Psi_q(\vec{x}, t_0), \quad (9)$$

with  $\Gamma_{sc} = \gamma_5$ . For the smearing functions  $\sigma_\alpha(\vec{x}_1 - \vec{x})$  we use a  $\delta$ -function local smearing ( $\alpha = 1$ ) or Gaussian smearings  $\propto e^{-|\vec{x}_1 - \vec{x}|^2/(2r_0^2)}$  for two different widths  $r_0$  and normalized to one ( $\alpha = 2, 3$ ). We then calculate a  $3 \times 3$  matrix of zero momentum meson correlators with all combinations of source and sink smearings,

$$C_{\beta,\alpha}^B(t, t_0) = \frac{1}{V} \sum_{\vec{x}} \sum_{\vec{y}} \langle \Phi_\beta^\dagger(\vec{y}, t) \Phi_\alpha(\vec{x}, t_0) \rangle, \quad (10)$$

with  $V = L^3$ . We use Gaussian widths in lattice units of size  $r_0 = 3$  or  $5$  on coarse ensembles and  $r_0 = 4$  or  $7$  on the fine ensembles. In addition to this matrix of  $B$  correlators we also need correlators with  $\Phi_\alpha$  at the source and  $J_0^{(i)}$  at the sink for  $i = 0, 1, 2$ ,

$$C_\alpha^{Ji}(t, t_0) = \frac{1}{V} \sum_{\vec{x}} \sum_{\vec{y}} \langle J_0^{(i)}(\vec{y}, t) \Phi_\alpha(\vec{x}, t_0) \rangle. \quad (11)$$

Since  $\gamma_0 \Psi_Q = \Psi_Q$  it turns out that

$$C_\alpha^{J0} \equiv C_{\beta=1,\alpha}^B, \quad (12)$$

Furthermore for zero momentum correlators one can show that

$$C_\alpha^{J2} \equiv C_\alpha^{J1}, \quad (13)$$

so only the three  $C_\alpha^{J1}$ ,  $\alpha = 1, 2, 3$ , are required in addition to the  $3 \times 3$  matrix  $C_{\beta,\alpha}^B$ .

The spatial sums  $\sum_{\vec{y}}$  in (10) and (11) are done at the sink, and so can be handled very easily. We implement the  $\sum_{\vec{x}}$  sums at the source via random wall sources. This is described for instance in Ref. [10]. Here we give some of the explicit formulas. In terms of quark propagators for the  $\Psi_Q$  and  $\Psi_q$  fields Eq. (10) becomes (we set  $t_0 = 0$  for simplicity)

$$\begin{aligned} C_{\beta,\alpha}^B(t) &= \frac{1}{V} \sum_{\vec{x}} \sum_{\vec{y}} \sum_{\vec{x}_1} \sum_{\vec{y}_1} \langle \text{tr} \{ G_Q(\vec{y}_1 - \vec{x}_1, t) \sigma_\alpha(\vec{x}_1 - \vec{x}) \\ &\quad \times \Gamma_{sc} G_q(\vec{x} - \vec{y}, -t) \Gamma_{sk} \sigma_\beta(\vec{y}_1 - \vec{y}) \} \rangle \\ &= \frac{1}{V} \sum_{\vec{x}} \sum_{\vec{y}} \sum_{\vec{x}_1} \sum_{\vec{y}_1} \langle \text{tr} \{ G_Q(\vec{y}_1 - \vec{x}_1, t) \sigma_\alpha(\vec{x}_1 - \vec{x}) \\ &\quad \times \Gamma_{sc} \gamma_5 G_q^\dagger(\vec{y} - \vec{x}, t) \gamma_5 \Gamma_{sk} \sigma_\beta(\vec{y}_1 - \vec{y}) \} \rangle. \end{aligned} \quad (14)$$

We set

$$G_Q^{(sm\alpha)}(\vec{y}_1, \vec{x}, t) \equiv \sum_{\vec{x}_1} G_Q(\vec{y}_1 - \vec{x}_1, t) \sigma_\alpha(\vec{x}_1 - \vec{x}), \quad (15)$$

and recall the relation between the naive HISQ propagator  $G_q(y - x)$  and the one component HISQ quark propagator  $G_\chi(y - x)$  [15],

$$G_q(y - x) = \Omega(y) G_\chi(y - x) \Omega^\dagger(x), \quad (16)$$

or equivalently,

$$G_q^\dagger(y - x) = \Omega(x) [\Omega(y) G_\chi(y - x)]^\dagger, \quad (17)$$

with,

$$\Omega(x) \equiv \gamma_0^{x_0} \gamma_1^{x_1} \gamma_2^{x_2} \gamma_3^{x_3}. \quad (18)$$

Setting  $\Gamma_{sc} = \Gamma_{sk} = \gamma_5$  one has

$$\begin{aligned} C_{\beta,\alpha}^B(t) &= \frac{1}{V} \sum_{\vec{x}} \sum_{\vec{y}} \sum_{\vec{y}_1} \langle \text{tr} \{ [G_Q^{(sm\alpha)}(\vec{y}_1, \vec{x}, t) \Omega(x)] [\Omega(y) \\ &\quad \times G_\chi(\vec{y} - \vec{x}, t)]^\dagger \sigma_\beta(\vec{y}_1 - \vec{y}) \} \rangle. \end{aligned} \quad (19)$$

We introduce a random U(1) field  $\xi(\vec{x})$  at each spatial site of the source time slice (in practice we employ separate U(1) fields for each color but suppress this index in the formulas given below) and replace

$$\frac{1}{V} \sum_{\vec{x}} \rightarrow \frac{1}{V} \sum_{\vec{x}} \sum_{\vec{x}'} \xi(\vec{x}) \xi^\dagger(\vec{x}'). \quad (20)$$

Equation (19) becomes

$$\begin{aligned} C_{\beta,\alpha}^B(t) &= \frac{1}{V} \sum_{\vec{x}} \sum_{\vec{x}'} \sum_{\vec{y}} \sum_{\vec{y}_1} \langle \text{tr} \{ [G_Q^{(sm\alpha)}(\vec{y}_1, \vec{x}, t) \Omega(x) \xi(\vec{x})] \\ &\quad \times [\Omega(y) G_\chi(\vec{y} - \vec{x}', t) \xi(\vec{x}')]^\dagger \sigma_\beta(\vec{y}_1 - \vec{y}) \} \rangle. \end{aligned} \quad (21)$$

An even more concise expression can be obtained if one defines

$$\begin{aligned} G_Q^{(sm\alpha, rw)}(\vec{y}_1, t) &\equiv \frac{1}{\sqrt{V}} \sum_{\vec{x}} G_Q^{(sm\alpha)}(\vec{y}_1, \vec{x}, t) \Omega(x) \xi(\vec{x}) \\ &= \frac{1}{\sqrt{V}} \sum_{\vec{x}_1} G_Q(\vec{y}_1 - \vec{x}_1, t) \\ &\quad \times \sum_{\vec{x}} \sigma_\alpha(\vec{x}_1 - \vec{x}) \Omega(x) \xi(\vec{x}), \end{aligned} \quad (22)$$

and,

$$\begin{aligned} G_q^{(rw)}(\vec{y}, t) &\equiv \Omega(y) G_\chi^{(rw)}(\vec{y}, t) \\ &\equiv \frac{1}{\sqrt{V}} \sum_{\vec{x}'} \Omega(y) G_\chi(\vec{y} - \vec{x}', t) \xi(\vec{x}'). \end{aligned} \quad (23)$$

This leads to

$$\begin{aligned} C_{\beta,\alpha}^B(t) &= \sum_{\vec{y}} \sum_{\vec{y}_1} \langle \text{tr} \{ [G_Q^{(sm\alpha, rw)}(\vec{y}_1, t)] \\ &\quad \times [G_q^{(rw)}(\vec{y}, t)]^\dagger \sigma_\beta(\vec{y}_1 - \vec{y}) \} \rangle. \end{aligned} \quad (24)$$

Equations (22) and (23) tell us that we should create NRQCD propagators with source,

$$SC_Q^\alpha(\vec{x}_1) = \frac{1}{\sqrt{V}} \sum_{\vec{x}} \sigma_\alpha(\vec{x}_1 - \vec{x}) \Omega(x) \xi(\vec{x}), \quad (25)$$

and HISQ propagators with source,

$$SC_q(\vec{x}') = \frac{1}{\sqrt{V}} \xi(\vec{x}'). \quad (26)$$

The double sum in (24) is carried out via fast Fourier transforms.

#### IV. FITS AND DATA ANALYSIS

The  $3 \times 3$  matrix of correlators  $C_{\beta,\alpha}^B$  of Eq. (10) and the  $C_\alpha^{J_i}$  of Eq. (11) for  $i = 1$  can be combined into a  $4 \times 3$  matrix of correlators  $C_{\beta,\alpha}$  with  $C_{\beta,\alpha} \equiv C_{\beta,\alpha}^B$  for  $\alpha, \beta = 1, 2, 3$  and  $C_{\beta=4,\alpha=1,2,3} \equiv C_{\alpha=1,2,3}^{J_1}$ . Various subsets of these correlators are then fit simultaneously to the form,

$$C_{\beta,\alpha}(t) = \sum_{j=0}^{N-1} b_j^\beta b_j^\alpha e^{-E_j(t-1)} + (-1)^t \sum_{k=0}^{\tilde{N}-1} \tilde{b}_k^\beta \tilde{b}_k^\alpha e^{-\tilde{E}_k(t-1)}, \quad (27)$$

to extract the ground state energy  $E_0$  and amplitudes  $b_0^\beta$ . The hadronic matrix elements appearing in (7) are related to the amplitudes  $b_0^\beta$  as

$$a^2 \langle 0 | J_0^{(0)} | B_q \rangle = \sqrt{2M_{B_q}} a b_0^{\beta=1} \quad (28)$$

and

$$a^2 \langle 0 | J_0^{(1)} | B_q \rangle = a^2 \langle 0 | J_0^{(2)} | B_q \rangle = \sqrt{2M_{B_q}} a b_0^{\beta=4}. \quad (29)$$

The factors of  $\sqrt{2M_{B_q}} a$  come about due to differences in normalization of states in the effective lattice theory compared to the standard relativistic normalization of states.

We have investigated fits to various subsets of correlators (submatrices) taken from the full  $4 \times 3$  matrix of 12 correlators. For each correlator we fit data between  $t = t_{\min}$  and  $t = t_{\max}$  with  $t_{\min} = 2 \sim 4$  and  $t_{\max} = 16$  on coarse ensembles and  $t_{\min} = 4 \sim 8$  and  $t_{\max} = 24$  on the fine ensembles. In Fig. 5 we show results for the  $B_s$  energy in lattice units,  $aE_{B_s}$ , from fits to ensemble C2. One sees a large improvement upon going from a fit to a single local-local ( $\alpha, \beta = 1$ ) correlator to a  $2 \times 2$  matrix of correlators ( $\alpha, \beta = 1, 2$  or  $\alpha, \beta = 1, 3$ ). There appears to be little further improvement when one goes to  $3 \times 3$  matrices. Our final fit results are taken from  $3 \times 2$  matrix fits with  $\alpha = 1, 3$  and  $\beta = 1, 3, 4$ . We do simultaneously a  $3 \times 2$  fit to  $B$  correlators together with a  $3 \times 2$  fit to  $B_s$  correlators. This allows us to get ratios such as  $f_{B_s} \sqrt{M_{B_s}} / f_B \sqrt{M_B}$  and mass differences such as  $M_{B_s} - M_B$  in a single fit with correctly correlated errors, in addition to the separate quantities  $f_B$  and  $f_{B_s}$ .

In all our fits we use Bayesian methods [16] and work with fixed  $t_{\min}$  and  $t_{\max}$  while increasing the number of

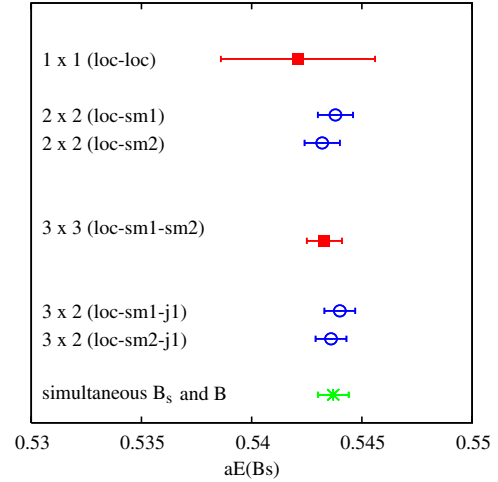


FIG. 5 (color online). Examples of results from different matrix fits for the  $B_s$  meson energy in lattice units. These fit results are taken from the C2 ensemble and used  $N = \tilde{N} = 7$  in Eq. (27).

exponentials  $N$  and  $\tilde{N}$  in Eq. (27) until fit results including errors and chisquares/degrees of freedom (DOF) have saturated. Figure 6 shows fit results for the  $B$  meson amplitude  $b_0^1$  on ensemble C1 versus  $N$  (which we also set equal to  $\tilde{N}$ ). One sees that things have stabilized by  $N = 4$ . In Table III we collect fit results for  $a^{3/2} \Phi \equiv a^{3/2} f_B \sqrt{M_B}$  and  $a^{3/2} \Phi_s \equiv a^{3/2} f_{B_s} \sqrt{M_{B_s}}$  for the six ensembles. The quantities  $\Phi^{(0)}$  and  $\Phi_s^{(0)}$  are analogous results if only the  $1 \times \langle J_0^{(0)} \rangle$  contribution is included on the right-hand side of Eq. (7), i.e., if one drops all one-loop and 1/M current corrections. In Table IV we summarize results for the mass difference  $\Delta M \equiv M_{B_s} - M_B$  in GeVs and the ratios  $\Phi_s / \Phi$  and  $\Phi_s^{(0)} / \Phi^{(0)}$ . Figure 4 illustrates the results for  $\Delta M$ . For the ratios one sees good agreement between

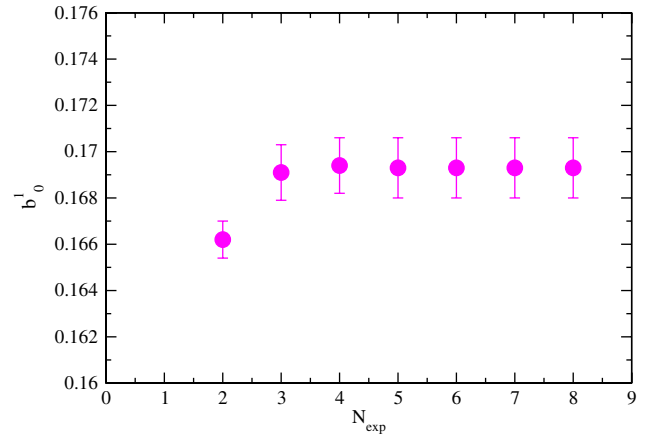


FIG. 6 (color online). Fit results for the  $B$  meson amplitude  $b_0^1$  on ensemble C1 versus the number of exponentials  $N = \tilde{N} \equiv N_{\text{exp}}$ . Simultaneous  $3 \times 2$  matrix fits were carried out to both  $B$  and  $B_s$  meson correlators at the same time.

TABLE III.  $\Phi \equiv f_B \sqrt{M_B}$  and  $\Phi_s \equiv f_{B_s} \sqrt{M_{B_s}}$  in lattice units. The lowest order results  $\Phi^{(0)}$  and  $\Phi_s^{(0)}$  are also shown. Errors include statistical and fitting errors.

Set	$a^{3/2}\Phi^{(0)}$	$a^{3/2}\Phi$	$a^{3/2}\Phi_s^{(0)}$	$a^{3/2}\Phi_s$
C1	0.2394(18)	0.2214(16)	0.2708(13)	0.2508(12)
C2	0.2498(18)	0.2313(17)	0.2780(9)	0.2577(8)
C3	0.2545(28)	0.2356(26)	0.2742(14)	0.2539(13)
F0	0.1431(16)	0.1293(14)	0.1647(8)	0.1489(7)
F1	0.1483(12)	0.1340(11)	0.1664(6)	0.1506(5)
F2	0.1520(12)	0.1375(10)	0.1656(7)	0.1498(6)

$\Phi_s/\Phi$  and  $\Phi_s^{(0)}/\Phi^{(0)}$  indicating complete lack of sensitivity to  $\mathcal{O}(\alpha)$  or  $\mathcal{O}(1/M)$  current corrections in this ratio.

## V. EXTRACTING CONTINUUM AND CHIRAL LIMIT PHYSICS

In this section we describe how we extract continuum and chiral limit physics from  $\Phi$ ,  $\Phi_s$  and  $\Phi_s/\Phi$  given in Tables III and IV. We fit  $\Phi$  and  $\Phi_s$  to the general form,

$$\Phi_q = \Phi_0(1 + \delta f_q + [\text{analytic}])(1 + [\text{discret}]), \quad (30)$$

(discret. being discretization) where  $\delta f_q$  includes the chiral logarithm terms. Explicit expressions, taken from the literature [17,18], are given in Appendix A. The chiral limit corresponds to  $m_l/m_s \rightarrow (m_l/m_s)_{\text{physical}} = 1/27.4$  together with  $m_s/m_c \rightarrow (m_s/m_c)_{\text{physical}} = 1/11.85$ . Most of our extrapolations employed formulas for  $\delta f_q$  at one-loop order in chiral perturbation theory (ChPT) and at lowest order in  $1/M$ . We have also included some  $1/M$  corrections such as effects of the  $B_q^*-B_q$  hyperfine splitting as discussed in Ref. [18]. For the [analytic] terms we use powers of  $m_{\text{valence}}/m_c$  and  $m_{\text{sea}}/\tilde{m}_c$ , where  $m_c$  is the bare HISQ charm quark mass (see Table II) fixed for each ensemble through the  $\eta_c$  mass, and  $\tilde{m}_c$  is the analogous bare AsqTad charm quark mass for  $\eta_c$  mesons made out of AsqTad quarks and antiquarks. The bare charm quark mass is a convenient scale to use since ratios such as  $m_s/m_c$  or  $m_l/m_c$  are equal to the corresponding ratio of  $\overline{MS}$  masses and are furthermore scale independent (up to discretization

TABLE IV.  $B_s$  and  $B$  mass difference  $\Delta M$ , and ratios  $\Phi_s^{(0)}/\Phi^{(0)}$  and  $\Phi_s/\Phi$ , with  $\Phi \equiv f_{B_q} \sqrt{M_{B_q}}$ . Errors include statistical and fitting errors.

Set	$\Delta M$ [GeV]	$\Phi_s^{(0)}/\Phi^{(0)}$	$\Phi_s/\Phi$
C1	0.0648(22)	1.1311(90)	1.1324(89)
C2	0.0577(18)	1.1132(65)	1.1143(64)
C3	0.0413(20)	1.0772(81)	1.0775(80)
F0	0.0717(29)	1.1508(123)	1.1516(121)
F1	0.0614(20)	1.1223(75)	1.1234(73)
F2	0.0478(13)	1.0889(51)	1.0896(50)

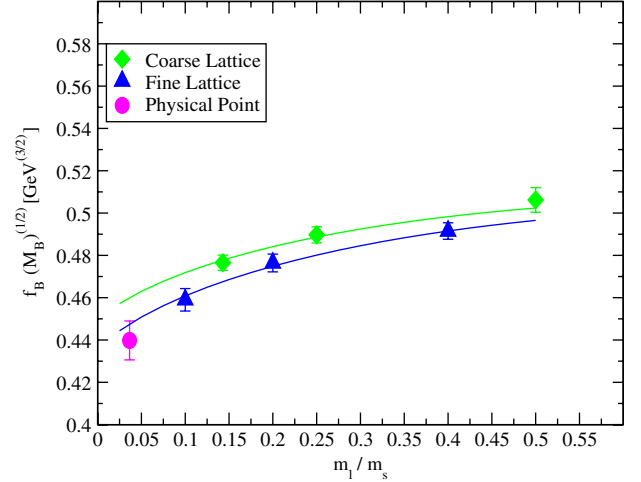


FIG. 7 (color online). Physical point extraction for  $\Phi = f_B \sqrt{M_B}$ .

corrections). The ratio  $\tilde{m}_c/m_c$  was found to be 0.9 in Ref. [7] for the fine ensembles. The same ratio will be approximately true for the coarse ensembles as well, since  $am_c$  does not vary too much for the lattice spacings employed here and mass renormalization starts only at order  $\alpha_s^2$ , with the one-loop corrections being very similar in the two actions.

For the [discret.] terms in (30) we employ powers of  $(a/r_1)^2$ . We allow for the expansion coefficients to be themselves functions of  $aM_b$  and/or  $am_q$  to take into account that we are dealing with an effective NRQCD theory for the  $b$ -quarks and with taste breaking splittings in staggered meson masses. With NRQCD  $b$ -quarks we cannot naively set  $a \rightarrow 0$ . What we do instead is fit the data to a theoretically motivated ansatz for discretization errors and then remove the latter. For instance with our current NRQCD action the leading order discretization errors go as  $a^2$  times a slowly varying function of  $aM_b$ . Reference [10] describes how we parameterize such  $aM_b$  dependence. This approach has worked well not just in the heavy-light spectroscopy calculations of Ref. [10] but also in recent HPQCD studies of  $\Upsilon$  physics with an improved NRQCD action [19]. In the present article we have tried ansätze for [discrete.] with both constant and  $aM_b$ -dependent coefficients multiplying powers of  $(a/r_1)$  and find little difference. This corresponds to test number 6 described below.

Figure 7 shows extraction of the physical point value (the magenta point) for  $\Phi_B$ . We show results using what we call our “basic” ansatz with

$$[\text{analytic}] = \beta_0(2m_u + m_s)/\tilde{m}_c + \beta_1 m_q/m_c + \beta_2(m_q/m_c)^2, \quad (31)$$

where  $m_u(m_q)$  denotes the sea (valence) light quark mass,

$$[\text{discret}] = c_0(a/r_1)^2 + c_1(a/r_1)^4, \quad (32)$$

and using (A7) from Appendix A for  $\delta f_q$ . The  $\chi^2/\text{DOF}$  for this fit was 0.24. We have checked the stability of our extractions by modifying the basic ansatz in the following ways:

- (1) dropping the  $\beta_2$  term in (31);
- (2) adding more  $(m_q/m_c)^n$  terms with  $n > 2$ ;
- (3) dropping the  $c_1$  term in (32);
- (4) adding more  $(a/r_1)^n$  terms with  $n > 4$ ;
- (5) making the coefficients  $c_i$  depend on  $m_q$ , i.e., a power series in  $m_q/m_c$ ;
- (6) making the coefficients  $c_i$  depend on  $aM_b$ ;
- (7) using (A1) rather than (A7) for  $\delta f_q$ ;
- (8) allowing for a 20% error in the scale  $f = f_\pi$  (see Appendix A for the relevant formulas).

Figure 8 summarizes results from these tests. We compare  $f_B$  at the physical point with these modifications in place with results obtained with the basic ansatz. The latter corresponds to the left most data point in Fig. 8 and is the same as the magenta point in Fig. 7. The integers on the horizontal axis in Fig. 8 refer to the type of modification of the basic ansatz as enumerated above. One sees that the basic ansatz result is very stable. The decay constant  $f_B$  changes by less than 1 MeV in all the tests undertaken.

In Figs. 9 and 10 we show physical point extractions for  $\Phi_s = f_{B_s} \sqrt{M_{B_s}}$  and  $\Phi_s/\Phi$  both carried out and tested along similar lines as for  $f_B$  in Figs. 7 and 8. The  $\chi^2/\text{DOF}$  for the two fits were 0.59 and 0.48 respectively.

The physical point results in Figs. 7 and 9 show statistical, extrapolation and  $r_1^{(3/2)}$  errors whereas in Fig. 10 only statistical and extrapolation errors are included. In the next section we will discuss additional systematic uncertainties inherent in our decay constant determinations.

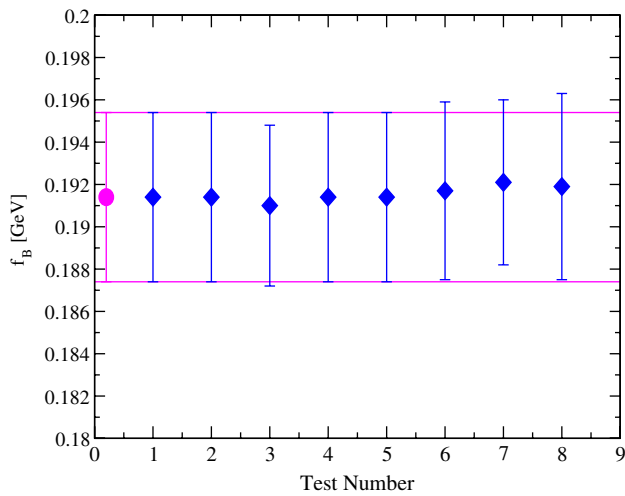


FIG. 8 (color online). Tests of  $f_B$  at the physical point. The left most magenta point is the “basic ansatz” result. The remaining points refer to results when the basic ansatz was modified in several ways as explained in the text.

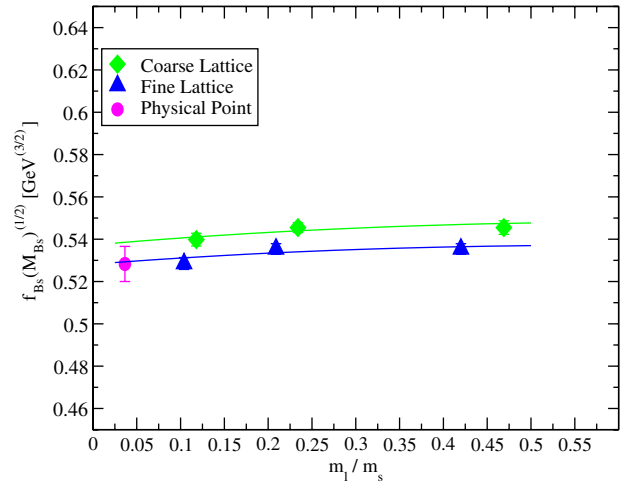


FIG. 9 (color online). Physical point extraction for  $\Phi_s = f_{B_s} \sqrt{M_{B_s}}$ .

## VI. RESULTS

Table V gives the error budget for  $f_B$ ,  $f_{B_s}$  and  $f_{B_s}/f_B$ . The first four entries, “statistical”, “scale  $r_1^{3/2}$ ”, “discretization corrections” and “chiral extrapolation and  $g_{B^*B\pi}$ ” are all part of the errors emerging automatically from the fits. Their individual contributions were separated out using the methods of Ref. [20] [see Eqs. (30) and (31) of that article]. The remaining four entries in Table V, “mass tuning,” “finite volume,” “relativistic corrections” and “operator matching” are additional systematic errors affecting our calculations. Sensitivity to the strange quark mass can be estimated by comparing results for valence quarks masses  $am_s$  and  $am_l$ . Similarly effects of mistuning of  $aM_b$  can be investigated using older NRQCD/HISQ decay constant results (see Ref. [21]) covering a range of  $aM_b$  values. Those calculations were done before proper retuning of the  $b$ -quark mass and provide information on how the decay constants depend on  $aM_b$ . For the finite volume uncertainty we take the same percentages as determined for the  $D$  and  $D_s$  meson decay constants in Ref. [22] using finite volume chiral perturbation theory. Our heavy-light currents have been matched to full QCD through order  $\alpha_s \Lambda_{\text{QCD}}/M_b$  and corrections come in at order  $(\Lambda_{\text{QCD}}/M_b)^2 \approx 0.01$ . There are order  $\alpha_s \Lambda_{\text{QCD}}/M_b$  corrections to the NRQCD action that are not included in our simulations. However, as discussed in Ref. [5], their effect on decay constants can be bounded to be at most  $\sim 1\%$ .

The  $O(\alpha_s^2)$  corrections to Eqs. (7) and (8) are not known. The  $J_0^{(i,\text{sub})}$  are nonleading, so the most important high-order correction is in the coefficient of  $J_0^{(0)}$ . To account for corrections at this level and beyond, we modify our data by multiplying the right-hand side of Eq. (7) by an overall factor of  $1 + \alpha_s^2 \rho'_0$  where we approximate  $\alpha_s^2 \approx 0.1$ . We use two different  $\rho'_0$ s, one for all coarse-lattice data and the



TABLE V. Error budget.

Source	$f_{B_s}$ (%)	$f_B$ (%)	$f_{B_s}/f_B$ (%)
Statistical	0.6	1.2	1.0
Scale $r_1^{3/2}$	1.1	1.1	-
Discretization corrections	0.9	0.9	0.9
Chiral extrapolation and $g_{B^*B\pi}$	0.2	0.5	0.6
Mass tuning	0.2	0.1	0.2
Finite volume	0.1	0.3	0.3
Relativistic corrections	1.0	1.0	0.0
Operator matching	4.1	4.1	0.1
Total	4.4	4.6	1.5

other for all fine-lattice data. To be conservative, we take each to be  $O(0.4)$ , which is more than twice as large as the one-loop  $\rho_0$  and also comparable to the estimates used in Ref. [5]: that is, we set each  $\rho'_0 = 0 \pm 0.4$ . The errors from these factors are combined in quadrature with the simulation errors in the currents, taking care to preserve the correlations caused by the fact that all course-lattice data has the same  $\rho'_0$ , as does all fine-lattice data. We then repeat the fits to Eq. (30) described in the previous section, this time applied to the modified data with enhanced errors. We use the difference between the total extrapolation error obtained with and without higher order matching errors added to the data to estimate the operator matching errors for  $f_B$  and  $f_{B_s}$ . These are given as the last entries in Table V. For the ratio  $f_{B_s}/f_B$ , matching errors are negligible, as was already pointed out at the end of Sec. IV.

Finally, we note that sea charm quarks are omitted in our simulations. However we expect their contributions to be small enough that the final total errors in Table V are unaffected.

Our final decay constant results including all the errors discussed above are

$$f_B = 0.191(9) \text{ GeV}, \quad (33)$$

$$f_{B_s} = 0.228(10) \text{ GeV}, \quad (34)$$

and

$$\frac{f_{B_s}}{f_B} = 1.188(18). \quad (35)$$

These numbers are in good agreement with HPQCD's previous NRQCD  $b$ -quark/AsqTad light quark results [5], however with improved total errors. Comparison plots are shown in the next section.

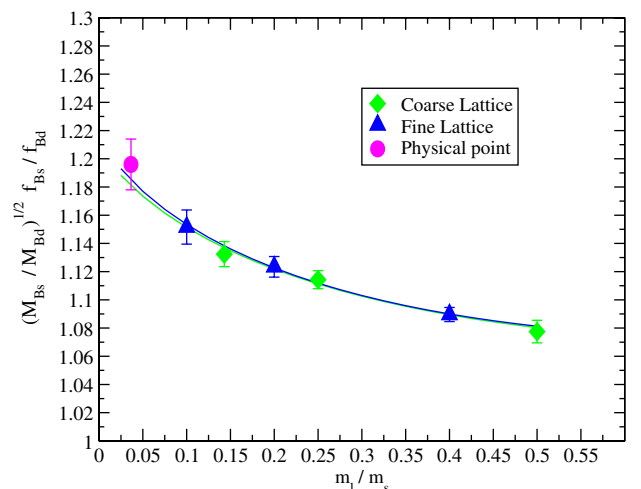
The errors in  $f_B$  and  $f_{B_s}$  are overwhelmingly dominated by the matching uncertainties. Without them, the total errors would be reduced to  $4.6\% \rightarrow 2.1\%$  and  $4.4\% \rightarrow 1.6\%$  for  $f_B$  and  $f_{B_s}$  respectively. Clearly a huge advantage can be gained if one could develop a formalism that did not require operator matching. One major motivation for designing the HISQ action [7] was to come up with a quark

action that could be used not only for accurate light quark physics, but also to simulate heavy quarks. It has been employed already very successfully for charmed quarks [11,22–24] and HPQCD has recently also started work with  $am_Q > am_c$  [25]. The HISQ action allows for a relativistic treatment of heavy quarks which means that one does not have to resort to effective theories. One important consequence is that decay constants can be determined from absolutely normalized currents. There is no need for operator matching. Furthermore it has been demonstrated that due to its high level of improvement the HISQ action can be used for heavy quarks up to about  $am_Q \leq 0.8$  without leading to large discretization effects. Recently a successful application of heavy HISQ quarks to  $B$  physics was achieved through a very accurate determination of the  $B_s$  meson decay constant, namely  $f_{B_s}^{(\text{HISQ})} = 0.225(4) \text{ GeV}$  with errors of only 1.8% [25]. There is very good agreement between  $f_{B_s}^{(\text{HISQ})}$  and the NRQCD  $b$ -quark result Eq. (34) of this article. This indicates that the very different systematic errors in the two calculations are under control and properly accounted for in our error estimates.

The HISQ  $b$ -quark calculation of  $f_{B_s}$  required going to very fine lattices including the MILC superfine and ultra-fine ensembles with lattice spacings  $\sim 0.06 \text{ fm}$  and  $\sim 0.045 \text{ fm}$  respectively. Repeating those calculations for the  $B$  meson with its light valence quark would be quite expensive and it will take some time before such calculations become available. In the mean time we can combine  $f_{B_s}^{(\text{HISQ})}$  with the result Eq. (35) of this article to extract a new and accurate  $f_B$ . One finds

$$\left[ \frac{f_{B_s}}{f_B} \right]_{\text{NRQCD}}^{-1} \times f_{B_s}^{(\text{HISQ})} \equiv f_B = 0.189(4) \text{ GeV}, \quad (36)$$

which is in excellent agreement with (33), only more accurate by better than a factor of 2. Equation (36) is the most important result of this article for phenomenology. It

FIG. 10 (color online). Physical point extraction for  $\Phi_s/\Phi$ .

also demonstrates the advantages of working with both HISQ and NRQCD  $b$ -quarks in parallel. In the future we plan to apply this combined approach to  $B$  and  $B_s$  semi-leptonic decay studies as well.

### VII. SUMMARY

We have carried out new determinations of  $f_B$ ,  $f_{B_s}$  and  $f_{B_s}/f_B$  using NRQCD  $b$ -quarks and HISQ light valence quarks and improve on our previous calculations with AsqTad light quarks. Figures 11–13, compare our new results with HPQCD’s older work [5,25] and also with results from the Fermilab/MILC [18] and the ETM [26] collaborations. One finds overall consistency between the different lattice groups. Our most accurate determination of  $f_B$ , Eq. (36), comes from combining the new ratio

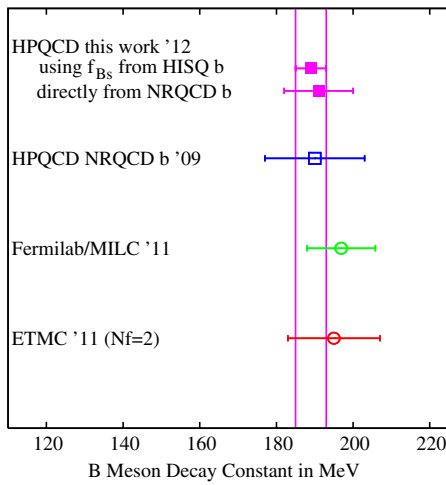


FIG. 11 (color online). Comparisons of results for  $f_B$  from this article with previous HPQCD work [5] and with results from the Fermilab/MILC [18] and ETM [26] collaborations.

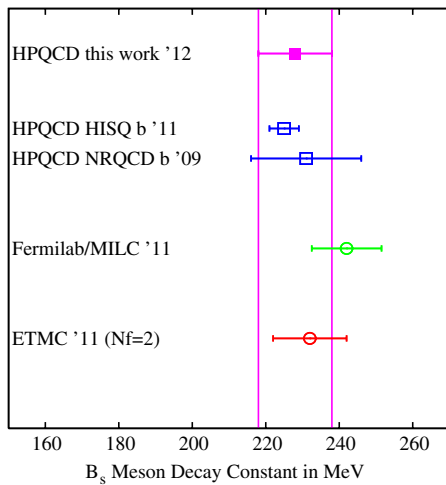


FIG. 12 (color online). Comparisons of results for  $f_{B_s}$  from this article with previous HPQCD work [5,25] and with results from the Fermilab/MILC [18] and ETM [26] collaborations.

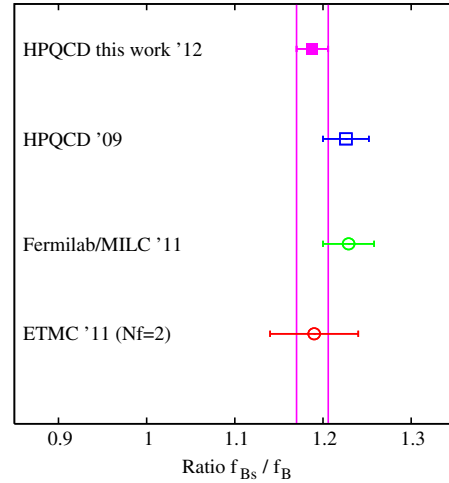


FIG. 13 (color online). Comparisons of results for  $f_{B_s}/f_B$  from this article with previous HPQCD work [5] and with results from the Fermilab/MILC [18] and ETM [26] collaborations.

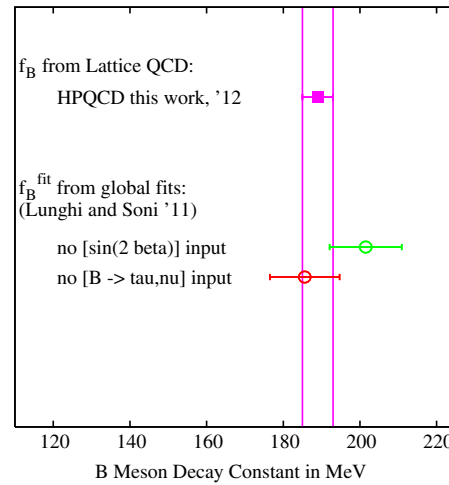


FIG. 14 (color online). Comparisons with  $f_B^{(\text{fit})}$  from global fits as given in Ref. [2].

$f_{B_s}/f_B$ , (35), with a precise determination of  $f_{B_s}$  based on HISQ  $b$ -quarks [25]. This gives the most precise  $f_B$  available today with errors of just 2.1%. As mentioned in Sec. I, accurate values for  $f_B$  are needed to compare with  $f_B^{(\text{fit})}$  from global fits in unitarity triangle analyses. In Fig. 14 we compare the new accurate  $f_B$  with two examples of  $f_B^{(\text{fit})}$  determined by Lunghi and Soni [2]. With current errors the two  $f_B^{(\text{fit})}$  values are consistent with each other and with  $f_B$  from lattice QCD. In the future, once errors are reduced considerably, these kind of comparisons could become more interesting.

### ACKNOWLEDGMENTS

This work was supported by the DOE (Grants No. DE-FG02-91ER40690, No. DE-FG02-04ER41302, and

No. DE-AC02-06CH11357), the NSF (Grant No. PHY-0757868), and the STFC. Numerical simulations were carried out on facilities of the USQCD collaboration funded by the Office of Science of the DOE and at the Ohio Supercomputer Center. Some calculations for this work were performed on the DiRAC facility jointly funded by the STFC and BIS. We thank the MILC collaboration for use of their gauge configurations.

## APPENDIX A: PARTIALLY QUENCHED CHPT CHIRAL LOGS

In this appendix we summarize partially quenched ChPT (PQChPT) expressions for the chiral logarithm terms  $\delta f_B$  and  $\delta f_{B_s}$ , taken from the literature. We follow closely the notation of Ref. [17] which we also adopted in our  $D \rightarrow K$  semileptonic paper [11]. We use “ $u$ ” and “ $s$ ” for sea and “ $q$ ” and “ $q_s$ ” for valence light and strange quarks respectively. Furthermore  $m_{ab}$  is the mass of the pseudoscalar meson with quark/antiquark content  $a$  and  $b$  and  $m_\eta^2 = \frac{1}{3}(m_{uu}^2 + 2m_{ss}^2)$ . For  $x = q$  or  $q_s$ , PQChPT gives

$$\delta f_{B_x} = \frac{1 + 3g^2}{32\pi^2 f^2} \left[ -2I_1(m_{xu}) - I_1(m_{xs}) - \frac{1}{3}DR^{[2,2]}(m_{xx}, I_1) \right], \quad (\text{A1})$$

where

$$I_1(m) = m^2 \log \frac{m^2}{\Lambda^2}, \quad (\text{A2})$$

and

$$DR^{[2,2]}(m; I) = \frac{\partial}{\partial m^2} R^{[2,2]}(m; I), \quad (\text{A3})$$

with

$$R^{[2,2]}(m; I) = \frac{(m_{uu}^2 - m^2)(m_{ss}^2 - m^2)}{(m_\eta^2 - m^2)} I(m) + \frac{(m_{uu}^2 - m_\eta^2)(m_{ss}^2 - m_\eta^2)}{(m^2 - m_\eta^2)} I(m_\eta). \quad (\text{A4})$$

In Eq. (A1)  $g$  is the  $B^*B\pi$  coupling which has not been measured yet experimentally, but for which several unquenched lattice determinations are now available [27]. We treat this “constant” as one of the fit parameters and set priors for the square of this coupling to a central value of  $g^2 = 0.25$  with width 0.10 (40%). This is consistent with typical values in the recent literature [27]. The scale  $\Lambda$  is set to  $4\pi f$ , with  $f$  given by the physical pion decay constant. In the full QCD limit the partially quenched formulas simplify to

$$\delta f_{B_s} = \frac{1 + 3g^2}{32\pi^2 f^2} \left[ -2I_1(m_K) - \frac{2}{3}I_1(m_\eta) \right], \quad (\text{A5})$$

$$\delta f_B = \frac{1 + 3g^2}{32\pi^2 f^2} \left[ -\frac{3}{2}I_1(m_\pi) - \frac{1}{6}I_1(m_\eta) - I_1(m_K) \right]. \quad (\text{A6})$$

Following Ref. [18] we have also considered PQChPT logs that include hyperfine and flavor splitting effects. A modification of the terms proportional to  $3g^2$  in (A1) is required leading to

$$\delta f_{B_x} = \frac{1}{32\pi^2 f^2} \left[ -2I_1(m_{xu}) - I_1(m_{xs}) - \frac{1}{3}DR^{[2,2]}(m_{xx}, I_1) + \frac{3g^2}{32\pi^2 f^2} \left[ -2J(m_{xu}, \Delta + \delta_{xu}) - J(m_{xs}, \Delta + \delta_{xs}) - \frac{1}{3}DR^{[2,2]}(m_{xx}, J(m_{xx}, \Delta)) \right] \right], \quad (\text{A7})$$

with

$$J(m, \Delta) = (m^2 - 2\Delta^2) \log \left( \frac{m^2}{\Lambda^2} \right) + 2\Delta^2 - 4\Delta^2 F(m/\Delta), \quad (\text{A8})$$

$$F(1/x) = \begin{cases} -\frac{\sqrt{1-x^2}}{x} \left[ \frac{\pi}{2} - \tan^{-1} \frac{x}{\sqrt{1-x^2}} \right] & |x| \leq 1 \\ \frac{\sqrt{x^2-1}}{x} \log(x + \sqrt{x^2-1}) & |x| \geq 1 \end{cases}. \quad (\text{A9})$$

$\Delta$  is the  $B_x^* - B_x$  hyperfine splitting and  $\delta_{xu}$  and  $\delta_{xs}$  adjust for the fact that in some one-loop diagrams the internal  $B_{u/s}^*$  does not have the same flavor as the external  $B_x$ . We have carried out chiral/continuum extrapolations with both (A1) and (A7). Differences in the final values at the physical point serve as a measure of systematic errors coming from our extrapolation ansatz.

## APPENDIX B: EXAMPLE OF PRIORS USED IN SEC. V

Table VI gives a sample set of priors and prior widths used for the  $f_B$  extraction in Sec. V. For parameters such as  $\beta_j$  or  $c_j$  where the overall sign is not known *a priori*, we

TABLE VI. Priors and prior widths for fits to Eq. (30).

	Prior	Width
$\Phi_0$	1.00	1.00
$\beta_0$	0.00	1.00
$\beta_1$	0.00	4.00
$\beta_2$	0.00	1.00
$c_0$	0.00	0.30
$c_1$	0.00	1.00
$g^2$	0.25	0.10
$r_1$	0.3133	0.0023

take the central value to be 0.0. The widths for the  $\beta_j$  depend on whether  $m_c$ ,  $1/a$  or  $1/r_1$  is used to set the scale for the masses. Although  $m_c$  is our preferred scale, due to the ease of handling quark mass running issues, we have also tried fits with the other scales and obtain consistent

results. In all cases fitted values for the parameters are consistent and within the widths assigned to them. For  $c_0$  we use prior widths of 0.3 to reflect the expectation that  $\mathcal{O}(a^2)$  errors come in as  $\mathcal{O}(\alpha_s a^2)$ . Again fit results for  $c_0$  are consistent with this expectation.

- 
- [1] E. Lunghi and A. Soni, *Phys. Lett. B* **697**, 323 (2011).
- [2] E. Lunghi and A. Soni, [arXiv:1104.2117](https://arxiv.org/abs/1104.2117).
- [3] A. Lenz *et al.* (CKMfitter Group), *Phys. Rev. D* **83**, 036004 (2011); J. Laiho, E. Lunghi, and R. Van De Water, Proc. Sci., FPCP2010 (2010) 040.
- [4] For some recent reviews, see R. Van de Water, Proc. Sci., LAT2009 (2009) 014; V. Lubicz, Proc. Sci., LAT2009 (2009) 013; J. Laiho, E. Lunghi, and R. S. Van de Water, *Phys. Rev. D* **81**, 034503 (2010); J. Shigemitsu, [arXiv:1102.0716](https://arxiv.org/abs/1102.0716); C. Davies, Proc. Sci., LATTICE2011 (2011) 019.
- [5] E. Gamiz *et al.* (HPQCD Collaboration), *Phys. Rev. D* **80**, 014503 (2009).
- [6] C. Bernard *et al.* (MILC Collaboration), *Phys. Rev. D* **64**, 054506 (2001).
- [7] E. Follana *et al.* (HPQCD Collaboration and UKQCD Collaboration), *Phys. Rev. D* **75**, 054502 (2007).
- [8] This article is part of HPQCD's program to study  $D$ ,  $D_s$ ,  $B$  and  $B_s$  decays and mixing on the MILC  $N_f = 2 + 1$  lattices with HISQ valence light, strange and charm quarks. Results for  $f_D$ ,  $f_{D_s}$ ,  $B$ ,  $B_s$  and  $B_c$  spectroscopy,  $m_s$ ,  $m_c$ ,  $m_b$ ,  $\alpha_s$ , and for  $D$  semileptonic form factors and  $V_{cd}$  and  $V_{cs}$  have already been published. This mixed action (HISQ valence on AsqTad sea) approach has also been tested through precision studies of light quark physics quantities such as  $f_\pi$  and  $f_K$ , where excellent agreement with experiment and results from nonmixed-action calculations (such as AsqTad on AsqTad) was found.
- [9] C. T. H. Davies *et al.* (HPQCD Collaboration), *Phys. Rev. D* **81**, 034506 (2010).
- [10] E. B. Gregory, C. T. H. Davies, I. D. Kendall, J. Koponen, K. Wong, E. Follana, E. Gamiz, G. P. Lepage *et al.*, *Phys. Rev. D* **83**, 014506 (2011).
- [11] H. Na, C. T. H. Davies, E. Follana, G. P. Lepage, and J. Shigemitsu, *Phys. Rev. D* **82**, 114506 (2010).
- [12] C. Monahan *et al.* (HPQCD Collaboration), to be published.
- [13] C. J. Morningstar and J. Shigemitsu, *Phys. Rev. D* **57**, 6741 (1998).
- [14] E. Dalgic, J. Shigemitsu, and M. Wingate, *Phys. Rev. D* **69**, 074501 (2004).
- [15] M. Wingate, J. Shigemitsu, C. T. H. Davies, G. P. Lepage, and H. D. Trotter, *Phys. Rev. D* **67**, 054505 (2003).
- [16] G. P. Lepage, B. Clark, C. T. H. Davies, K. Hornbostel, P. B. Mackenzie, C. Morningstar, and H. Trotter, *Nucl. Phys. B, Proc. Suppl.* **106–107**, 12 (2002).
- [17] C. Aubin and C. Bernard, *Phys. Rev. D* **73**, 014515 (2006).
- [18] A. Bazavov *et al.* (Fermilab Lattice Collaboration and MILC Collaboration), *Phys. Rev. D* **85**, 114506 (2012).
- [19] R. J. Dowdall *et al.* (HPQCD Collaboration), *Phys. Rev. D* **85**, 054509 (2012).
- [20] C. T. H. Davies *et al.* (HPQCD Collaboration), *Phys. Rev. D* **78**, 114507 (2008).
- [21] J. Shigemitsu *et al.* (HPQCD Collaboration), Proc. Sci., LAT2009 (2009) 251, see Fig. 3 of this article.
- [22] E. Follana *et al.* (HPQCD Collaboration and UKQCD Collaboration), *Phys. Rev. Lett.* **100**, 062002 (2008).
- [23] H. Na, C. T. H. Davies, E. Follana, J. Koponen, G. P. Lepage, and J. Shigemitsu, *Phys. Rev. D* **84**, 114505 (2011).
- [24] C. T. H. Davies, C. McNeile, E. Follana, G. P. Lepage, H. Na, and J. Shigemitsu, *Phys. Rev. D* **82**, 114504 (2010).
- [25] C. McNeile, C. T. H. Davies, E. Follana, K. Hornbostel, and G. P. Lepage, *Phys. Rev. D* **85**, 031503 (2012).
- [26] P. Dimopoulos *et al.* (ETM Collaboration), *J. High Energy Phys.* **01** (2012) 046.
- [27] W. Detmold, C.-J. D. Lin, and S. Meinel, *Phys. Rev. D* **85**, 114508 (2012); H. Ohki, H. Matsufuru, and T. Onogi, *Phys. Rev. D* **77**, 094509 (2008); D. Becirevic, B. Blossier, E. Chang, and B. Haas, *Phys. Lett. B* **679**, 231 (2009); J. Bulava *et al.* (ALPHA Collaboration), Proc. Sci., LATTICE2010 (2010) 303.